Supplemental material for "Electric Hall Effect and Quantum Electric Hall Effect"

Chaoxi Cui,[1,2,3] Run-Wu Zhang,[1,2,3,*] Yuhui Qiu,[1,2,3] Yilin Han,[1,2,3] Zhi-Ming Yu,[1,2,3,†] and Yugui Yao[1,2,3,‡]

[1] *Centre for Quantum Physics, Key Laboratory of Advanced Optoelectronic Quantum Architecture and Measurement (MOE), School of Physics, Beijing Institute of Technology, Beijing 100081, China*
[2] *Beijing Key Lab of Nanophotonics & Ultrafine Optoelectronic Systems, School of Physics, Beijing Institute of Technology, Beijing 100081, China*
[3] *Beijing Institute of Technology, Zhuhai, 519000, China*

I. CONCRETE CANDIDATE MATERIALS

After introducing the concepts of electric Hall effect (EHE) and quantum electric Hall effect (QEHE), we illustrate our main ideas with two concrete candidate materials. In this work, we focus on layered alkaline-earth metal-decorated transition metal (TM) nitrides, *viz.* $Ca(FeN)_2$ (mp-1423472), and a derivative of $Ba_2Mg(VS_3)_2$ (mp-2217817), *viz.* $Ba_2Mg(MnS_3)_2$, which are proposed in the Materials Projection (https://materialsproject.org).

We take monlayer $Ca(FeN)_2$ as an example to verify the feasibility of the material. For further checking the stability of monolayer $Ca(FeN)_2$, thermal stability is examined using ab initio molecular dynamics (AIMD) with 3×3 supercells at 100 K. The snapshots of structure for monolayer $Ca(FeN)_2$ at 100 K is shown in Fig. S1. After running for 5 ps, no bond is obviously broken, although each lattice exhibited various degrees of distortion. Overall, the result suggests that monolayer $Ca(FeN)_2$ can maintain good thermal stability.

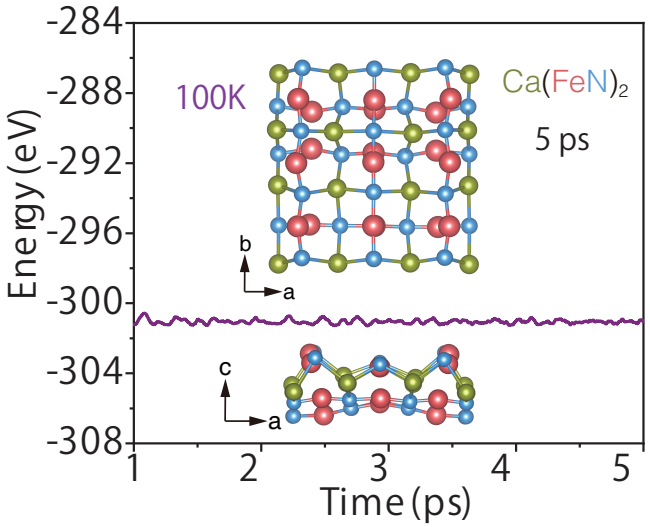

FIG. S1: (Color online) As a typical example of testing thermal stability, herein, the total energies with AIMD simulation of the monolayer $Ca(FeN)_2$ are calculated under 100 K. Thereinto, the snapshots of the crystal structures after 5 ps in the insets.

To explore the intriguing physical properties of monolayer $Ca(FeN)_2$ and monolayer $BaMn_2S_3$, understanding their magnetic ground states is essential. Here, we investigate two possible types of magnetic ordering, specifically antiferromagnetic Néel order (AFM-Néel) and ferromagnetic (FM), in accordance with the crystal structure depicted in Fig. S2. Our analysis demonstrates that the AFM-Néel state has a lower energy than the FM state, suggesting that monolayer $Ca(FeN)_2$ and monolayer $BaMn_2S_3$ tend toward AFM ground states (referred to Table S1 and Table S2 for details). Moreover, we find that the AFM-Néel ground state with out-of-plane spin direction in $Ca(FeN)_2$ remains stable with variations in U from 3.5 eV up to 4 eV. Calculations of magnetocrystalline anisotropy energy (MAE) at

* zhangrunwu@bit.edu.cn
† zhiming_yu@bit.edu.cn
‡ ygyao@bit.edu.cn

a U value of 3 eV indicates that $Ca(FeN)_2$ behaves as a soft altermagnet, with a maximum MAE value of 0.131 meV per unit cell. Regarding monolayer $BaMn_2S_3$, it is observed that the AFM-Néel ground state with out-of-plane spin orientation in monolayer $BaMn_2S_3$ maintains stability with U value 3.5 eV. MAE calculations with a U value of 3 eV shows that monolayer $BaMn_2S_3$ also displays property of a soft altermagnet, with a small MAE value of 0.036 meV per unit cell. For soft altermagnet case, the magnetic characteristics of monolayer $Ca(FeN)_2$ and monolayer $BaMn_2S_3$ can be manipulated by changing the magnetization direction from out-of-plane to in-plane.

Given that the candidate materials studied all contain transition metal (TM) atoms with strongly correlated $3d$ electrons, we adopt Hubbard U with moderate values for $3d$ TM atoms to check our results. To fully validate our ideas, we test several U values including 3 eV, 3.5 eV and 4 eV, as shown in Fig. S3 and Fig. S4. Notably, the key band features remain robust over a wide range of Hubbard U values. Increasing the U value mainly resulted in increased band gaps.

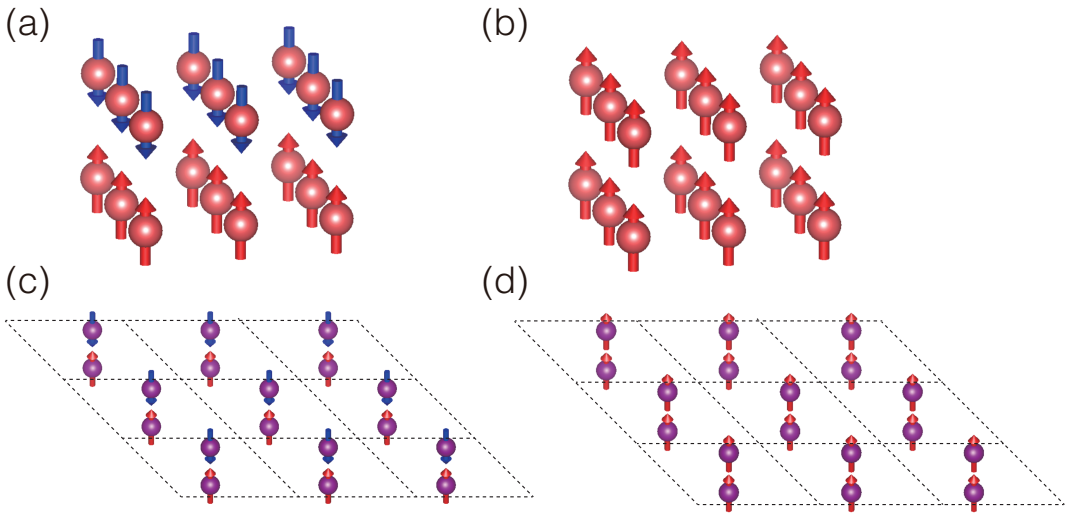

FIG. S2: (Color online) To better check magnetic ground states of monolayer $Ca(FeN)_2$ and monolayer $BaMn_2S_3$, we examined two different types of feasible magnetic orders, including (a) and (c) antiferromagnetic Néel order (AFM-Néel), (b)and (d) ferromagnetic (FM). Here, the magnetic structures are examined using a 3×3 supercell.

TABLE S1: Considering different Hubbard U values, the relative energies (in unit of eV/Fe atom) for (a) A-type AFM, (b) FM orders in the supercell of $Ca(FeN)_2$ are listed in the following table. The ΔE_{MAE} (in unit of meV/unit cell) is defined as the difference of total energy between in-plane and out-of-plane spin directions, *i.e.*, $\Delta E_{MAE} = E(\theta = 90°, \phi = 0°) - E(\theta = 0°, \phi = 0°)$. Here, $E(\theta, \phi)$ is the total energy when the spin points to the direction labeled by the polar (θ) and azimuthal (ϕ) angles. The positive (negative) value indicates a favored out-of-plane (in-plane) magnetization.

Hubbard U value (eV)	AFM	FM	ΔE_{MAE}
3	0	0.00595	-0.131
3.5	0	0.00834	4.217
4	0	0.01204	2.706

TABLE S2: Considering different Hubbard U values, the relative energies (in unit of eV/Mn atom) for (a) A-type AFM, (b) FM orders in the supercell of $BaMn_2S_3$ are listed in the following table. The ΔE_{MAE} (in unit of meV/unit cell) is defined as the difference of total energy between in-plane and out-of-plane spin directions, *i.e.*, $\Delta E_{MAE} = E(\theta = 90°, \phi = 0°) - E(\theta = 0°, \phi = 0°)$. Here, $E(\theta, \phi)$ is the total energy when the spin points to the direction labeled by the polar (θ) and azimuthal (ϕ) angles. The positive (negative) value indicates a favored out-of-plane (in-plane) magnetization.

Hubbard U value (eV)	AFM	FM	ΔE_{MAE}
3	0	0.03151	-0.109
3.5	0	0.01412	0.418

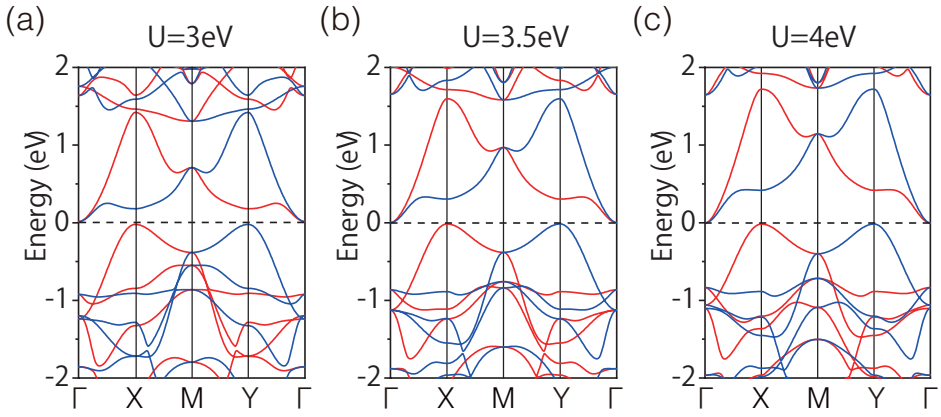

FIG. S3: (Color online) Spin-resolved band structures of monolayer $Ca(FeN)_2$ in absence of SOC effect with different U values, including U=3 eV (a), U=3.5 eV (b), and U=4 eV (c). Red and blue lines represent spin-up and spin-down channels, respectively.

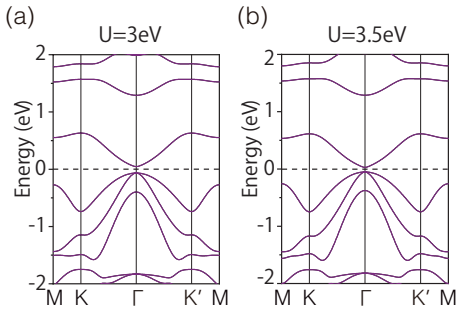

FIG. S4: (Color online) Band structures of monolayer $BaMn_2S_3$ in absence of SOC effect with different U values, including U=3 eV (a), U=3.5 eV (b).

II. LIST OF EHE-COMPATIBLE MAGNETIC POINT (LAYER) GROUPS

Based on the symmetry requirements detailed in Table I in the main text, we identified all magnetic point groups (MPGs) and magnetic layer groups (MLGs) that are compatible with EHE, as shown in Table S3. This identification significantly simplifies the search for suitable materials and provides valuable guidance for classifying potentially feasible materials. We have determined that 62 of the 528 MLGs are compatible with EHE.

TABLE S3: List of magnetic point groups and the magnetic layer group that permit EHE. The symmetries belong to $M_z\mathcal{TS}$ which is critical for EHE , are presented in second column.

MPG	$M_z\mathcal{TS}$	MLG	MPG	$M_z\mathcal{TS}$	MLG
$\bar{1}'$	$P\mathcal{T}$	2.3.6	$4/m'$	$S_{4z}\mathcal{T}, P\mathcal{T}$	51.3.364,52.3.371
m'	$M_z\mathcal{T}$	4.3.14 5.3.19	422	$C_{2\parallel}$	53.1.374,54.1.381
$2/m'$	$P\mathcal{T}$	6.4.24,7.4.31,14.3.68,15.3.78,	$\bar{4}'2m'$,$\bar{4}'m'2$	$S_{4z}\mathcal{T}, C_{2\parallel}$	57.4.401,58.4.408 ,59.5.414,60.5.421
		16.3.85,17.3.92,18.3.97	$4/m'm'm'$	$S_{4z}\mathcal{T}, C_{2\parallel}, P\mathcal{T}$	61.3.424,62.3.437,63.3.446,64.3.455
2	$C_{2\parallel}$	8.1.34,9.1.41,10.1.45	$\bar{3}'$	$S_{3z}\mathcal{T}, P\mathcal{T}$	66.3.466
222	$C_{2\parallel}$	19.1.104,20.1.111,21.1.118,22.1.122	321	$C_{2\parallel}$	68.1.470
$m'2m'$	$C_{2\parallel}, M_z\mathcal{T}$	27.3.156,28.3.169,29.3.176,30.3.183	$\bar{3}'1m'$,$\bar{3}'m'1$	$S_{3z}\mathcal{T}, C_{2\parallel}, P\mathcal{T}$	71.3.481 ,72.3.486
		31.3.190,32.3.199,33.3.204	$\bar{6}'$	$S_{6z}\mathcal{T}, M_z\mathcal{T}$	74.3.494
		34.3.209,35.3.214,36.3.223	$6/m'$	$S_{6z}\mathcal{T}, M_z\mathcal{T}, P\mathcal{T}$	75.3.497
$m'm'm'$	$C_{2\parallel}, P\mathcal{T}$	37.3.232,38.3.245,39.3.258,40.3.265	622	$C_{2\parallel}$	76.1.500
		41.3.278,42.3.291,43.3.300,44.3.309	$\bar{6}'m'2$,$\bar{6}'2m'$	$S_{6z}\mathcal{T}, M_z\mathcal{T}, C_{2\parallel}$	78.5.514 ,79.4.518
		45.3.316,46.3.325,47.3.332,48.3.345	$6/m'm'm'$	$S_{3z}\mathcal{T}, C_{2\parallel}, P\mathcal{T}, M_z\mathcal{T}$	80.3.522
$\bar{4}'$	$S_{4z}\mathcal{T}$	50.3.360			

III. DERIVATION OF EHE COEFFICIENT

When $\mathcal{E}_z$ is finite but weak, the Hamiltonian of the perturbed system reads

$$\hat{H} = \hat{H}_0 + g_E\mathcal{E}_z\hat{z}. \tag{S1}$$

According to the standard perturbation theory [6], the $\mathcal{E}_z$ has a linear correction on both band dispersion and wave function of system, expressed as

$$\tilde{\epsilon}_n = \epsilon_n + P_{nn}\mathcal{E}_z, \tag{S2}$$

$$|\tilde{u}_n\rangle = |u_n\rangle + \mathcal{E}_z\sum_{l\neq n}\frac{P_{ln}}{\epsilon_n-\epsilon_l}|u_l\rangle, \tag{S3}$$

where $P_{nm} = g_E\langle u_n(\boldsymbol{k})|\hat{z}|u_m(\boldsymbol{k})\rangle$ and $u_n(\boldsymbol{k})$ is unperturbed wave function. Then the perturbed Berry curvature $\tilde{\Omega}_n(\boldsymbol{k})$ can be expressed as

$$\tilde{\Omega}_n(k) = -2\mathrm{Im}\sum_{m\neq n}\frac{\langle\tilde{u}_n|\hat{v}_x|\tilde{u}_m\rangle\langle\tilde{u}_m|\hat{v}_y|\tilde{u}_n\rangle}{(\tilde{\epsilon}_m-\tilde{\epsilon}_n)^2}, \tag{S4}$$

where velocity element of the perturbed system to the first order of $\mathcal{E}_z$ is

$$\langle\tilde{u}_n|\hat{v}_{x(y)}|\tilde{u}_m\rangle = \langle u_n|\hat{v}_{x(y)}|u_m\rangle + \mathcal{E}_z\sum_{l\neq n}\frac{P^*_{ln}}{\varepsilon_n-\varepsilon_l}\langle u_l|\hat{v}_{x(y)}|u_m\rangle + \mathcal{E}_z\sum_{l\neq m}\frac{P_{lm}}{\varepsilon_m-\varepsilon_l}\langle u_n|\hat{v}_{x(y)}|u_l\rangle. \tag{S5}$$

Then, each term in the perturbed Berry curvature is obtained as

$$\begin{aligned}\frac{\langle\tilde{u}_n|\hat{v}_x|\tilde{u}_m\rangle\langle\tilde{u}_m|\hat{v}_y|\tilde{u}_n\rangle}{(\tilde{\epsilon}_m-\tilde{\epsilon}_n)^2} &= \frac{v_x^{nm}v_y^{mn}}{(\varepsilon_m-\varepsilon_n)^2} - 2\mathcal{E}_z\frac{P_{mm}-P_{nn}}{(\varepsilon_m-\varepsilon_n)^3}v_x^{nm}v_y^{mn} \\ &+ \mathcal{E}_z\sum_{l\neq m}\frac{P_{lm}v_x^{nl}v_y^{mn}+P^*_{lm}v_x^{nm}v_y^{ln}}{(\epsilon_n-\epsilon_m)^2(\epsilon_m-\epsilon_l)} + \mathcal{E}_z\sum_{l\neq n}\frac{P^*_{ln}v_x^{lm}v_y^{mn}+P_{ln}v_x^{nm}v_y^{ml}}{(\epsilon_n-\epsilon_m)^2(\epsilon_n-\epsilon_l)}\end{aligned} \tag{S6}$$

where only the terms up to the first order of $\mathcal{E}_z$ are kept. Consequently, we have

$$\tilde{\Omega}_n(\boldsymbol{k}) = \Omega_n(\boldsymbol{k}) + \Lambda_n(\boldsymbol{k})\mathcal{E}_z, \tag{S7}$$

with $\Omega_n(\boldsymbol{k}) = -2\mathrm{Im}\sum_{m\neq n}\frac{v_x^{nm}v_y^{mn}}{(\varepsilon_m-\varepsilon_n)^2}$, and

$$\Lambda_n(\boldsymbol{k}) = -2\mathrm{Im}\sum_{m\neq n}\left[-2\frac{P_{mm}-P_{nn}}{(\varepsilon_m-\varepsilon_n)^3}v_x^{nm}v_y^{mn}+\sum_{l\neq m}\frac{P_{lm}^*v_y^{ln}v_x^{nm}+P_{lm}v_x^{nl}v_y^{mn}}{(\varepsilon_n-\varepsilon_m)^2(\varepsilon_m-\varepsilon_l)}+\sum_{l\neq n}\frac{P_{ln}v_y^{ml}v_x^{nm}+P_{ln}^*v_x^{lm}v_y^{mn}}{(\varepsilon_n-\varepsilon_m)^2(\varepsilon_n-\varepsilon_l)}\right]. \tag{S8}$$

In the semi-classical approach, the current of electrons is given by

$$\boldsymbol{j} = -e\int_k\frac{d^2k}{(2\pi)^2}\sum_n\tilde{f}_n(\tilde{\varepsilon}_n)\tilde{\boldsymbol{v}}_n, \tag{S9}$$

where n denotes the n-th band and $\tilde{f}_n$ is the Fermi-Dirac distribution of the n-th band. The group velocity $\tilde{\boldsymbol{v}}_n$ is given by

$$\begin{aligned}\tilde{\boldsymbol{v}}_n &= \frac{1}{\hbar}\nabla_{\boldsymbol{k}}\tilde{\varepsilon}_n-\frac{e}{\hbar}\boldsymbol{E}\times\tilde{\boldsymbol{\Omega}}_{\boldsymbol{n}} \\ &= \frac{1}{\hbar}\nabla_{\boldsymbol{k}}\varepsilon_n+\frac{1}{\hbar}\mathcal{E}_z\nabla_{\boldsymbol{k}}P_{nn}-\frac{e\boldsymbol{E}}{\hbar}\times\boldsymbol{\Omega}_{\boldsymbol{n}}-\mathcal{E}_z\frac{e\boldsymbol{E}}{\hbar}\times\boldsymbol{\Lambda}_n,\end{aligned} \tag{S10}$$

where $\boldsymbol{E}$ is the in-plane driving field. Next we consider the semi-classical Boltzmann equation of electrons

$$\partial_t\tilde{f}-\frac{e\boldsymbol{E}}{\hbar}\cdot\nabla_{\boldsymbol{k}}\tilde{f}+\boldsymbol{v}\nabla_{\boldsymbol{r}}\tilde{f}=\mathcal{I}(\tilde{f}), \tag{S11}$$

where $\mathcal{I}(f)$ is scattering term. After applying the relaxation time approximation and assuming $\tilde{f}$ is spatially uniform and the system is in its equilibrium, the Boltzmann equation becomes

$$-\frac{e\boldsymbol{E}}{\hbar}\cdot\nabla_{\boldsymbol{k}}\tilde{f}(\tilde{\varepsilon}_n) = \frac{\tilde{f}_n(\tilde{\varepsilon}_n)-f(\tilde{\varepsilon}_n)}{\tau}. \tag{S12}$$

To the leading order of τ, $\boldsymbol{E}$ and $\mathcal{E}_z$, we arrive at

$$\begin{aligned}\tilde{f}(\tilde{\varepsilon}_n) &= f(\tilde{\varepsilon}_n)-\frac{e\tau}{\hbar}\left(\boldsymbol{E}\cdot\nabla_{\boldsymbol{k}}\tilde{\varepsilon}_n\right)\frac{\partial f\left(\varepsilon_n\right)}{\partial\varepsilon_n} \\ &= f\left(\varepsilon_n\right)+\frac{\partial f\left(\varepsilon_n\right)}{\partial\epsilon_n}P_{nn}\mathcal{E}_z-\frac{e\tau}{\hbar}\left(\boldsymbol{E}\cdot\nabla_{\boldsymbol{k}}\varepsilon_n+\mathcal{E}_z\boldsymbol{E}\cdot\nabla_{\boldsymbol{k}}P_{nn}\right)\frac{\partial f\left(\varepsilon_n\right)}{\partial\epsilon_n}.\end{aligned} \tag{S13}$$

Substituting Eq. (S10) and Eq. (S13) into Eq. (S9), we can arrive at the current proportional to $\boldsymbol{E}\mathcal{E}_z$:

$$\begin{aligned}\boldsymbol{j} &= \frac{e^2\tau}{\hbar}\mathcal{E}_z\int_k\frac{d^2k}{(2\pi)^2}\sum_n\frac{\partial f\left(\varepsilon_n\right)}{\partial\epsilon_n}\left[\frac{1}{\hbar}\nabla_{\boldsymbol{k}}P_{nn}\left(\boldsymbol{E}\cdot\nabla_{\boldsymbol{k}}\varepsilon_n\right)+\frac{1}{\hbar}\nabla_{\boldsymbol{k}}\varepsilon_n\left(\boldsymbol{E}\cdot\nabla_{\boldsymbol{k}}P_{nn}\right)\right] \\ &+\frac{e^2}{\hbar}\mathcal{E}_z\int_k\frac{d^2k}{(2\pi)^2}\sum_n\frac{\partial f\left(\varepsilon_n\right)}{\partial\epsilon_n}P_{nn}\left(\boldsymbol{E}\times\boldsymbol{\Omega}_{\boldsymbol{n}}\right)+f\left(\varepsilon_n\right)\left(\boldsymbol{E}\times\boldsymbol{\Lambda}_n\right).\end{aligned} \tag{S14}$$

For 2D systems, we have $\boldsymbol{E}=(E_x,E_y,0)$, $\boldsymbol{\Omega}_{\boldsymbol{n}}=(0,0,\Omega_n)$ and $\boldsymbol{\Lambda}_n=(0,0,\Lambda_n)$. Thus, the total EHE coefficient (including intrinsic and extrinsic parts) $\chi_{ab}^{\mathrm{ex+in}}$ is obtained as

$$\chi_{ab}^{\mathrm{ex+in}} = \frac{j_a}{E_b\mathcal{E}_z}=\chi_{ab}^{\mathrm{in}}+\chi_{ab}^{\mathrm{ex}}, \tag{S15}$$

with

$$\chi_{ab}^{\mathrm{in}} = \epsilon_{ab}\frac{e^2}{\hbar}\int\frac{d^2k}{(2\pi)^2}\sum_n\left[\frac{\partial f\left(\varepsilon_n\right)}{\partial\epsilon_n}P_{nn}\Omega_n+f\left(\varepsilon_n\right)\Lambda_n\right], \tag{S16}$$

and

$$\chi_{ab}^{\mathrm{ex}} = \tau\frac{e^2}{\hbar^2}\int\frac{d^2k}{(2\pi)^2}\sum_n\frac{\partial f\left(\varepsilon_n\right)}{\partial\epsilon_n}\frac{\partial^2}{\partial_a\partial_b}\left(P_{nn}\varepsilon_n\right), \tag{S17}$$

where $\{a,b\} \in \{x,y\}$ and ϵ_{ab} is Levi-Civita symbol. The first term ($\chi_{ab}^{\rm in}$) is the intrinsic EHE coefficient, which has been presented in main text as Eq. (6). The second term ($\chi_{ab}^{\rm ex}$) has a dependence on the relaxing time τ, corresponding to the extrinsic EHE coefficient. It is easy to note that the intrinsic term is antisymmetric, due to the Levi-Civita symbol ($\epsilon_{ab} = -\epsilon_{ba}$), while the extrinsic term is symmetric as $\frac{\partial^2}{\partial_a \partial_b} = \frac{\partial^2}{\partial_b \partial_a}$. Strictly speaking, the extrinsic EHE is not a Hall effect, as it is not antisymmetric.

Next, we present a symmetry analysis for extrinsic EHE. Similar to the intrinsic EHE, the extrinsic EHE also requires $\sigma_{ab}^{\rm ex} = 0$ ($\sigma_{ab}^{\rm ex} \propto \tau$) and $\chi_{ab}^{\rm ex} \neq 0$ ($\chi_{ab}^{\rm ex} \propto \tau$). Following the analysis in the main text, we can also decompose magnetic layer-point-group symmetry operators into $\mathcal{O}$ and $M_z\mathcal{O}$, where $\mathcal{O} = \left\{E, C_{2,z}, C_{n,z}, M_\parallel\right\} \otimes \{E, \mathcal{T}\}$ (with $n = 3, 4, 6$). $\mathcal{O}$ can be further subdivided into $\mathcal{O} = R_1 + R_2$. $R_1 = \{E, C_{2z}\} \otimes \{E, \mathcal{T}\}$, which allows both $\sigma_{ab}^{\rm ex}$ and $\chi_{ab}^{\rm ex}$. In contrast, $R_2 = \{C_{nz}, M_\parallel\} \otimes \{E, \mathcal{T}\}$, which forbids both $\sigma_{ab}^{\rm ex}$ and $\chi_{ab}^{\rm ex}$, as here $\sigma_{ab}^{\rm ex}$ and $\chi_{ab}^{\rm ex}$ are symmetric. Due to the same reason discussed in the main text, $M_zR_1(M_zR_2)$ annihilates (allows) $\chi_{ab}^{\rm ex}$. Therefore, we can obtain the symmetry requirements of extrinsic EHE: for a system hosting extrinsic EHE, it should have no symmetries in R_2 or M_zR_1 while it must have at least one symmetry in M_zR_2. The symmetries in R_1 are optional. The results of the symmetry analysis are summarized in Table. S4.

TABLE S4: Symmetry requirements of the extrinsic EHE. "✓" and "✗" denote that the element is symmetry allowed and forbidden, respectively. Notice that $n = 3, 4, 6$ in $C_{n,z}$ and $S_{n,z}$.

	R_1	R_2	M_zR_1	M_zR_2
Elements	$\{E, C_{2z}\} \otimes \{E, \mathcal{T}\}$	$\{C_{nz}, M_\parallel\} \otimes \{E, \mathcal{T}\}$	$\{M_z, \mathcal{P}\} \otimes \{E, \mathcal{T}\}$	$\{S_{nz}, C_{2,\parallel}\} \otimes \{E, \mathcal{T}\}$
$\sigma_{ab}^{\rm ex}$	✓	✗	✓	✗
$\chi_{ab}^{\rm ex}$	✓	✗	✗	✓
Requirement	optional	forbidden	forbidden	requisite

IV. EFFECTIVE $\mathcal{T}$ SYMMETRY IN COLLINEAR OR COPLANAR MAGNETIC MATERIALS

When spin degree of freedom is considered but the SOC effect is ignored, the symmetry of the systems should be described by spin space group [7–12], the operator of which is generally written as

$$g = \{U \| R | \boldsymbol{\tau}\}, \tag{S18}$$

where U acts on spin, R acts on lattice and $\boldsymbol{\tau}$ is translation. For collinear or coplanar magnetic materials, they all have an operator: $\{C_{2\perp}\mathcal{T} \| E | 0\}$. Here, $C_{2\perp}$ stands for a 180 degree rotation along axis normal to the direction of all spins in the system. Since $\{C_{2\perp}\mathcal{T} \| E | 0\}$ does not exchange the spin index and the $C_{2\perp}$ only acts on spin, the system should have an effective $\mathcal{T}$ symmetry. Thus, there will not be either anomalous Hall effect or intrinsic EHE in collinear and coplanar magnetic materials without SOC.

[1] J. P. Perdew, K. Burke, and M. Ernzerhof, Generalized gradient approximation made simple, Phys. Rev. Lett. **77**, 3865 (1996).
[2] P. E. Blöchl, Projector augmented-wave method, Phys. Rev. B **50**, 17953 (1994).
[3] V. I. Anisimov, Vi anisimov, j. zaanen, and ok andersen, phys. rev. b 44, 943 (1991)., Phys. Rev. B **44**, 943 (1991).
[4] A. A. Mostofi, J. R. Yates, Y.-S. Lee, I. Souza, D. Vanderbilt, and N. Marzari, wannier90: A tool for obtaining maximally-localised wannier functions, Comput. Phys. Commun. **178**, 685 (2008).
[5] Q. Wu, S. Zhang, H.-F. Song, M. Troyer, and A. A. Soluyanov, Wanniertools: An open-source software package for novel topological materials, Comput. Phys. Commun. **224**, 405 (2018).
[6] F. M. Fernández, *Introduction to perturbation theory in quantum mechanics* (CRC press, 2000).
[7] W. Brinkman and R. J. Elliott, Theory of spin-space groups, Proceedings of the Royal Society of London. Series A. Mathematical and Physical Sciences **294**, 343 (1966).
[8] D. B. Litvin and W. Opechowski, Spin groups, Physica **76**, 538 (1974).
[9] P. Liu, J. Li, J. Han, X. Wan, and Q. Liu, Spin-group symmetry in magnetic materials with negligible spin-orbit coupling, Physical Review X **12**, 021016 (2022).
[10] Z. Xiao, J. Zhao, Y. Li, R. Shindou, and Z.-D. Song, Spin space groups: Full classification and applications, Physical Review X **14**, 031037 (2024).
[11] X. Chen, J. Ren, Y. Zhu, Y. Yu, A. Zhang, P. Liu, J. Li, Y. Liu, C. Li, and Q. Liu, Enumeration and representation theory of spin space groups, Physical Review X **14**, 031038 (2024).

[12] Y. Jiang, Z. Song, T. Zhu, Z. Fang, H. Weng, Z.-X. Liu, J. Yang, and C. Fang, Enumeration of spin-space groups: Toward a complete description of symmetries of magnetic orders, Physical Review X **14**, 031039 (2024).